TU Delft

Delft University of Technology

D-Decomposition Based Robust Discrete-Time Current Regulator for Grid-Connected VSI

Tyuryukanov, I.; Popov, M.

DOI
10.1109/ISIE45063.2020.9152394

Publication date
2020

Document Version
Final published version

Published in
29th IEEE International Symposium on Industrial Electronics

Citation (APA)
Tyuryukanov, I., & Popov, M. (2020). D-Decomposition Based Robust Discrete-Time Current Regulator for Grid-Connected VSI. In *29th IEEE International Symposium on Industrial Electronics : 17-19 June 2020, online conference hosted in Delft, The Netherlands* (pp. 100-107). Article 9152394 IEEE. https://doi.org/10.1109/ISIE45063.2020.9152394

Important note
To cite this publication, please use the final published version (if applicable).
Please check the document version above.

Copyright
Other than for strictly personal use, it is not permitted to download, forward or distribute the text or part of it, without the consent of the author(s) and/or copyright holder(s), unless the work is under an open content license such as Creative Commons.

Takedown policy
Please contact us and provide details if you believe this document breaches copyrights.
We will remove access to the work immediately and investigate your claim.

This work is downloaded from Delft University of Technology.
For technical reasons the number of authors shown on this cover page is limited to a maximum of 10.

Green Open Access added to TU Delft Institutional Repository

'You share, we take care!' - Taverne project

https://www.openaccess.nl/en/you-share-we-take-care

Otherwise as indicated in the copyright section: the publisher is the copyright holder of this work and the author uses the Dutch legislation to make this work public.

D-Decomposition Based Robust Discrete-Time Current Regulator for Grid-Connected VSI

Ilya Tyuryukanov*, Marjan Popov

Faculty of EEMCS, Delft University of Technology, Delft, Netherlands
email: ilya.tyuryukanov@ieee.org

***Abstract*—The D-decomposition method allows to design control structures with prescribed locations of closed loop poles. Unlike the root locus method, D-decomposition natively handles two variable regulator parameters, which makes it suitable for more complex control structures. Moreover, an extension to more than two variable parameters is straightforward. In this paper, the advantages of the D-decomposition method are illustrated by synthesizing a robust low-order current regulator for a grid-connected voltage source inverter (VSI) with LCL filter. It is shown how to visualize the complete region in the low dimensional regulator parameter space satisfying certain robust performance criteria (with robust stability being a special case). The paper concludes by simulation results validating the robustness properties of the designed low-order regulator under substantial grid impedance variations.**

***Index Terms*—Current control, D-decomposition, LCL-filter, robust stability, robust performance**

I. Introduction

Nowadays, the increasing economical and environmental concerns are enabling the transition from fossil power plants towards renewable power generation, primarily from photovoltaic (PV) and wind turbine (WT) systems. An increasing amount of energy is being generated locally by distributed generation (DG) systems that interface PV and WT sources with the electric grid by means of a pulse-width modulation (PWM) voltage source inverters (VSI). A classic issue in the control of VSI-based DG systems is the damping of resonance peaks of LC and LCL filters. The LC or LCL filters are most commonly used in VSI-based DG systems because they provide a higher attenuation of switching harmonics for the same value of filter inductances, thus considerably saving the VSI weight and cost. However, the resonance peaks of these filter types require a special treatment to ensure a good closed-loop stability. Another common issue is the possibility of DG operation in remote areas with weak grid connection. Because of it, DG manufactures have to consider the uncertainty of the equivalent grid impedance at the point of common coupling (PCC) of VSI with the grid.

The topic of robust current regulator design for LCL-VSI has gained a considerable attention in the literature. Oftentimes, the desired robustness is achieved by applying the techniques from nonlinear [1] or optimal robust control [2], [3]. The resulting regulators may often be non-standard and of a high order. However, industry manufacturers tend to favor proven standard low-order regulator types (e.g., PI or PR regulators) due to their clarity and ease of maintenance. To address this demand, multiple works propose to robustify the familiar loop shaping technique from classic control theory [4], [5]. However, the robustification guidelines based on phase and gain margins are usually empiric do not explicitly relate the plant uncertainty and the closed-loop control performance.

This paper proposes a novel approach to tackle uncertain grid equivalents at the PCC that is based on D-decomposition [6]–[8]. By applying D-decomposition to the control of VSI with LCL output filters, it becomes possible to simultaneously tune the gains of the proportional LCL resonance damping and proportional-resonant (PR) current reference tracking regulators. The use of D-decomposition and other parametric methods for the purpose of robustness analysis and robust controller synthesis has been popularized by Ackerman as *parameter space approach* to control design [9]. However, the practical implementation aspects of both D-decomposition and the parameter space approach are usually not discussed in the existing literature. This paper aims to fill this gap by describing both the robust current regulation methodology for VSI-interfaced DG and its possible implementation as a software tool[1]. Some desirable numerical improvements are discussed as well.

In Section II, the VSI control task is introduced. The D-decomposition method is summarized in Section III, and Section IV describes its application to the design of robust controllers. Section V describes the implementation of the techniques from Sections III–IV. Section VI contains time-domain simulation results and illustrates one possible extension of the proposed techniques. Conclusions and possible improvements are summarized in Section VII.

II. Current Regulation of VSI with LCL Filter

The selected VSI current regulation structure is shown in Figure 1. It consists of two feedback loops [10]. The inner loop is the capacitor current feedback with proportional gain k_{ic}. Its goal is the stability enhancement by damping the resonance of the LCL output filter consisting of two inductances L_1 and L_2, and capacitor C_{x1}. The parasitic resistances R_1, R_2, and R_{x1} are shown for completeness. Capacitor current i_c is obtained as difference between VSI output current i_1 and grid current

[1]The MATLAB codes accompanying this paper are available at `https://github.com/ityuryukanov/dd`.

978-1-7281-5635-4/20/$31.00 ©2020 IEEE

Authorized licensed use limited to: TU Delft Library. Downloaded on August 13,2020 at 09:18:18 UTC from IEEE Xplore. Restrictions apply.

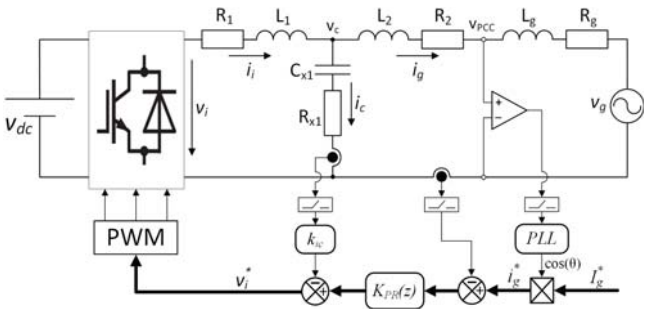

Fig. 1: Double-loop VSI current regulation structure

i_g. Due to its high harmonic content, current i_1 is sampled synchronously with the PWM carrier waveform [10].

The outer control loop is the grid current feedback with PR regulator $K_{PR}(z)$. Its goal is tracking of the grid current reference i^*_{out} and rejection of disturbances caused by variations of grid voltage v_g. The grid is represented by its Thévenin equivalent at the PCC consisting of voltage v_g behind grid inductance L_g and grid resistance R_g.

The continuous-time plant model (i.e., the LCL filter and grid impedance) can be derived in its state-space form by considering the VSI output voltage v_i and grid back emf v_g as system inputs. For a discrete-time control implementation, all feedback and control signals are sampled with zero-order hold (ZOH). Therefore, the plant model should be discretized into the z-domain by using the ZOH method. The continuous-time PR regulator model [11] is discretized with the Tustin method with prewarping around the resonance frequency ω_r:

$$
\begin{aligned}
&K_{PR}(s) = k_p + K_R(s) \rightarrow K_{PR}(z) = k_p + K_R(z)\\
&K_R(s) = \frac{k_r\omega_c s}{s^2 + 2\omega_c s + \omega_r^2} \rightarrow K_R(z) = \frac{b_2 z^2 + b_1 z + b_0}{a_2 z^2 + a_1 z + a_0}\\
&b_2 = k_r\omega_c \sin(\omega_r T_s);\ a_2 = 2\omega_r + 2\omega_c \sin(\omega_r T_s);\\
&b_1 = 0;\ a_1 = -4\omega_r \cos(\omega_r T_s);\\
&b_0 = -k_r\omega_c \sin(\omega_r T_s);\ a_0 = 2\omega_r - 2\omega_c \sin(\omega_r T_s);
\end{aligned}
\tag{1}
$$

where k_p is the proportional gain, $K_R(s)$ is the resonant term of $K_{PR}(s)$, and T_s is the sampling period. Multiplier ω_c shifts the resonant poles of $K_R(s)$ left from the imaginary axis to avoid instability due to round-off errors in coefficients. The resonant gain k_r influences the frequency bandwidth of high gains around ω_r. In (1), $K_R(s)$ consists of a single term with ω_r equal to the nominal grid frequency ω_0. However, extra resonant terms can be added in parallel at frequencies of typical low-frequency harmonics (e.g., 5^{th}, 7^{th} etc.) to improve their rejection. Parameters k_r and ω_c of $K_{PR}(s)$ have a limited impact on closed-loop stability by mostly affecting the performance around ω_r (i.e., *not* around the crossover frequency). Therefore, the only control parameters that significantly affect the system stability are k_p and k_{ic}. All other fixed system parameters are given in Table I.

In Table I, V_n and f_0 are the grid rated voltage and nominal frequency, f_{sw} and f_s are the VSI switching frequency and

TABLE I: Fixed System Parameters

Parameters	Value
V_n, f_0	400 V, 50 Hz
VSI rated power	21 kVA
V_{dc}	700 V
L_1, R_1, C_{x1}, R_{x1}	1.6 mH, 2 mΩ, 10 μF, 0.1 mΩ
L_2, R_2	0.8 mH, 1 mΩ
f_{sw}, f_s	8 kHz, 16 kHz
PWM type	sinusoidal PWM (SPWM)
k_r, ω_c, ω_r	30, 3 rad/s, 2π50 rad/s

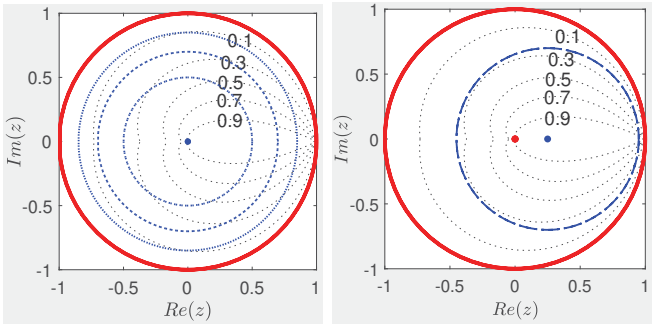

(a) Settling time boundaries (b) Damping & settling time boundary

Fig. 2: Boundaries of various transfer function pole regions

controller sampling frequency. The LCL filter parameters have been computed based on [12]. Parameters k_r and ω_c are set through tuning the control performance specifically for 50 Hz signals. The inverter topology is modeled as a two level half-bridge.

III. D-DECOMPOSITION METHOD

D-decomposition allows to analyze the dependence of stability and control performance of a linear dynamic system from its two parameters. These two varying parameters must enter linearly into the system characteristic polynomial. For the control problem in Figure 1, its closed-loop characteristic polynomial can be separated into three terms based on the most influential control parameters k_p and k_{ic}:

$$D(z) = k_p U(z) + k_{ic} V(z) + W(z) \tag{2}$$

Since closed-loop poles are the *roots* of the corresponding characteristic polynomial, a characterization of roots of $D(z)$ in (2) is of interest.

A. Specification of Root Boundaries

The mapping of system poles from the s-domain to the discrete-time z-domain is described by the relationship $z = \exp(s/f_s)$, where s is the complex frequency and f_s is the sampling frequency of the discrete-time system. By substituting $z = \exp(j\omega/f_s)$, $\omega \in (-\infty, \infty)$, the s-domain stability boundary (i.e., the imaginary axis) is mapped into the z-domain. This is the traditional choice for D-decomposition [6], but not the only possible one [9].

Often it is desirable to satisfy some control performance requirements beyond the closed-loop stability. For example, it

Authorized licensed use limited to: TU Delft Library. Downloaded on August 13,2020 at 09:18:18 UTC from IEEE Xplore. Restrictions apply.

is possible to reduce the settling time of a dynamic system by constraining the real parts of all of its poles not to exceed a certain value. For an underdamped second order system, the output settles to ± 5 % of its steady-state value within the time $t_{s,5\%}$ if the real parts of system poles do not exceed $\sigma^* = -3/t_{s,5\%}$ [13]. In s-domain, this corresponds to the root boundary $s = \sigma^* + j\omega$. Its mapping to the z-plane is defined by $z = \exp\left((\sigma^* + j\omega)/f_s\right)$, or $z = \exp\left(\sigma^*/f_s\right)\exp\left(j\omega/f_s\right)$, which describes a set of circles centered at the origin with radius less than 1 (see Figure 2a and [9]).

Many sources address the mapping of lines of equal damping from the s-plane into the discrete time domain (e.g., [9], [13]), and the constant damping *contours* can be visualized in MATLAB [14] by the command `zgrid()`. In Figure 2b, the damping contour $\zeta = 0.3$ is approximated by a circle of radius 0.7 with its center shifted right from the origin by 0.25 [9]. From Figures 2a–2b, the boundaries of closed-loop poles in terms of system damping and settling time can be reasonably approximated by circles of varying radii and center:

$$z = R \cdot \exp(j\Omega) + \delta \tag{3}$$

where R is the circle radius, $\delta \in \mathbb{R}$ is the shift from the origin, and $\Omega \in [-\pi, \pi]$ is equivalent to ω/f_s, $\omega \in (-\infty, \infty)$.

By setting $R = 1$ and $\delta = 0$ in (3), z is constrained to the discrete-time stability boundary (red in Figure 2). The chosen circular contour (3) can be plugged into the characteristic polynomial in (2) by considering (3) as polynomial $z = R \cdot x + \delta$, which implies $z^n = (R \cdot x + \delta)^n$, which can be expanded either through polynomial multiplication by using Fast Fourier Transform (FFT) or through the binomial theorem.

B. Mapping of Root Boundaries into Two Parameter Plane

The main idea of D-decomposition is to map the root boundaries on the z-plane described in Section III-A into the plane of two system parameters (i.e., the *parameter plane*). This is achieved by plugging the contour equation (3) into (2), which results in a *complex trigonometric polynomial* [9]:

$$D'(\Omega) = k_p U'(\Omega) + k_{ic} V'(\Omega) + W'(\Omega) \tag{4}$$

where $U'(\Omega) = \sum_{n=1}^{p} U'_n \cdot \exp(jn\Omega)$, and $V'(\Omega)$, $W'(\Omega)$ are of the same form as $U'(\Omega)$. Separating the real and imaginary parts, while aiming to find the zeros of (4) yields:

$$\begin{cases} k_p U'_{re}(\Omega) + k_{ic} V'_{re}(\Omega) + W'_{re}(\Omega) = 0 \\ k_p U'_{im}(\Omega) + k_{ic} V'_{im}(\Omega) + W'_{im}(\Omega) = 0 \end{cases} \tag{5}$$

where $U'_{re}(\Omega)$, $V'_{re}(\Omega)$, $W'_{re}(\Omega)$ are finite linear combinations of $\cos(n\Omega)$, $n \in \mathbb{N}$, and $\Omega \in [0, \pi]$. Similarly, $U'_{im}(\Omega)$, $V'_{im}(\Omega)$, $W'_{im}(\Omega)$ are finite linear combinations of $\sin(n\Omega)$. Note that considering $\Omega \in [0, \pi]$ instead of $\Omega \in [-\pi, \pi]$ is correct because all system eigenvalues are symmetrical about the real axis.

The linear combinations of $\cos(n\Omega)$, $\sin(n\Omega)$ in (5) are known as *real trigonometric polynomials* [9], and they are closely related to the *Chebyshev polynomials*. Therefore, it is possible to convert (5) into regular polynomials by using the substitution $\cos(\Omega) = x$ and the Chebyshev polynomials of the first (for U'_{re}, V'_{re}, W'_{re}) and second (for U'_{im}, V'_{im}, W'_{im}) kind, with the new variable $x \in [-1,\ 1]$:

$$\begin{cases} k_p U''_{re}(x) + k_{ic} V''_{re}(x) + W''_{re}(x) = 0 \\ \sqrt{1-x^2}(k_p U''_{im}(x) + k_{ic} V''_{im}(x) + W''_{im}(x)) = 0 \end{cases} \tag{6}$$

The next step is to solve (6) for k_p and k_{ic}. This is done by using the Cramer's rule to write the determinants of (6) and the expressions for $k_p(x)$ and $k_{ic}(x)$, $x \neq \pm 1$:

$$\begin{aligned} & k_p(x) = \frac{\Delta_1(x)}{\Delta_0(x)}; \quad k_{ic}(x) = \frac{\Delta_2(x)}{\Delta_0(x)}; \\ & \frac{\Delta_1(x)}{\Delta_0(x)} = \begin{vmatrix} -W''_{re}(x) & V''_{re}(x) \\ -W''_{im}(x) & V''_{im}(x) \end{vmatrix} \Big/ \begin{vmatrix} U''_{re}(x) & V''_{re}(x) \\ U''_{im}(x) & V''_{im}(x) \end{vmatrix} \\ & \frac{\Delta_2(x)}{\Delta_0(x)} = \begin{vmatrix} U''_{re}(x) & -W''_{re}(x) \\ U''_{im}(x) & -W''_{im}(x) \end{vmatrix} \Big/ \begin{vmatrix} U''_{re}(x) & V''_{re}(x) \\ U''_{im}(x) & V''_{im}(x) \end{vmatrix} \end{aligned} \tag{7}$$

Substituting $x \in [-1,\ 1]$ into (7) produces the mapping of the root boundaries (3) into the plane of parameters k_{ic} and k_p. The characterization of $k_p(x)$ and $k_{ic}(x)$ by (7) results in zero values of (4), i.e. for any (k_p, k_{ic})-pair satisfying (7) some system poles lie on the specified contour (3). Therefore, the parametric curves $k_p(x)$ and $k_{ic}(x)$ divide the $k_{ic}0k_p$ plane into sectors with equal counts of closed-loop eigenvalues outside of the specified contour (3).

When calculating the borders of *root invariant regions* according to (7), three cases are possible for every x:

$\Delta_0(x) \neq 0$: The linear system of equations in (6) has solution and $k_p(x)$, $k_{ic}(x)$ can be calculated according to (7).

$\Delta_0(x) = 0 \wedge (\Delta_1(x) \neq 0 \vee \Delta_2(x) \neq 0)$: The system in (6) has no solutions. At such x both $k_p(x)$ and $k_{ic}(x)$ go to infinity, and it looks like a discontinuity on the solution graph.

$\Delta_0(x) = 0 \wedge (\Delta_1(x) = 0 \wedge \Delta_2(x) = 0)$: The solutions of system in (6) are represented by a straight line $k_p U''_{re}(x_{sng}) + k_{ic} V''_{re}(x_{sng}) + W''_{re}(x_{sng}) = 0$, where x_{sng} are such that $\Delta_0(x_{sng}) = 0 \wedge \Delta_1(x_{sng}) = 0 \wedge \Delta_2(x_{sng}) = 0$.

Therefore, it is very important to determine the values of x at which the determinant $\Delta_0(x)$ is zero. The permanent singular x are[2] $x_{sng} = -1$ and $x_{sng} = 1$, but for some specific problems there may be more singularities. At this point, the advantage of using polynomials in x becomes more obvious, as it is possible to find all roots of a regular polynomial as the eigenvalues of its companion matrix. Moreover, computing the determinants in (7) involves pairwise products of functions. If the two functions are polynomials, their product can be computed as discrete convolution of their coefficient vectors.

C. An Illustrative Example

In Figure (3), a possible outcome of applying the methods of Sections III-A and III-B to the VSI current regulation problem in Section II is illustrated. The mapped root boundary in (3) is $R = 0.987$ and $\delta = 0$, which translates into the requirement

[2]Since sine equations for $U'_{im}(\Omega)$, $V'_{im}(\Omega)$, $W'_{im}(\Omega)$ are all equal to zero for $\Omega = \pi k,\ k \in \mathbb{Z}$, which is reflected by the $\sqrt{1-x^2}$ factor in (6).

Authorized licensed use limited to: TU Delft Library. Downloaded on August 13,2020 at 09:18:18 UTC from IEEE Xplore. Restrictions apply.

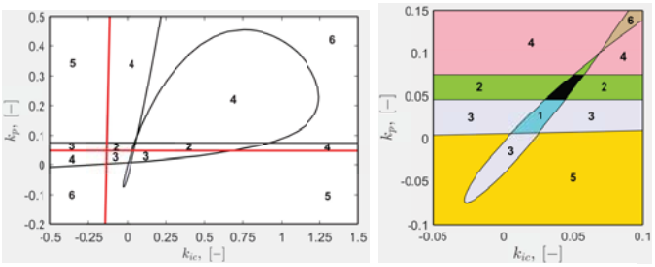

(a) CRB and RRB curves (b) Enlarged Γ-stable region

Fig. 3: Root invariant regions for $L_g = 0$, $R_g = 0$

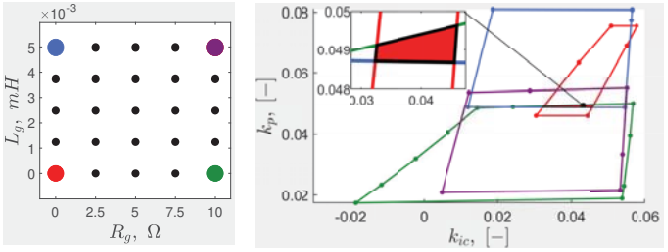

(a) Uncertainty set (b) Robust region $t_{s,5\%} \leq 14.3$ ms

Fig. 4: Γ-stable root invariant regions for $z = 0.987\exp(j\Omega)$

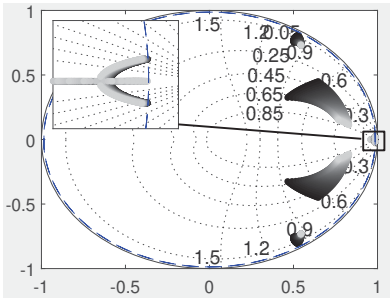

Fig. 5: Closed-loop poles with fixed $K_{PR}(z)$

of $t_{s,5\%} \leq 14.3$ ms, and the grid equivalent is assumed equal to $L_g = 0$ mH, $R_g = 0\ \Omega$.

In Figure (3a), the two red lines represent the singular case $x_{sng} = \pm 1$, and they are often called the *real root boundaries* (RRBs). For the considered control problem, there are no other x_{sng} besides ± 1 (the typical situation). The curve (7) is drawn in black color for $x : \Delta_0(x) \neq 0$. This curve is often called the *complex root boundary* (CRB). The meaning of the terms RRB and CRB is explained in many sources related to parametric control (e.g., [7], [9]).

As mentioned in Section III-B, the RRB lines and CRB curves shown in Figure 3a form the boundaries of root invariant regions in the plane $k_{ic}0k_p$. It is enough to take a single point inside of a region to check for the whole region the number of closed-loop system poles outside of the root boundary (3). Choosing $z = \exp(j\Omega)$ as the root boundary is done to search for the root invariant regions that ensure the closed-loop stability (i.e., zero poles outside of the unity circle). Analogously, a generic root boundary inside of $z = \exp(j\Omega)$ (e.g., see Figure 2) poses a stricter requirement on the closed-loop poles that is known as Γ-*stability* [9]. The Γ-stable region for the Γ-stability specification $z = 0.987 \cdot \exp(j\Omega)$ is shown in Figure 3b as the black-filled region.

IV. Parameter Space Approach

The parameter space approach, as introduced in English control literature by Ackermann (e.g., see [9]), has two major steps. In the *controller synthesis step*, root invariant regions satisfying certain closed-loop pole specifications (3) are computed in the domain of variable regulator parameters for several uncertain plant representatives. The crossing of the Γ-stable regions defines the set of robust regulator candidates. In the *control loop analysis step*, the candidate controller is analyzed for the whole uncertainty range to verify its robust Γ-stability. If the candidate controller ensures the required closed-loop pole specifications for the whole uncertainty range, then the design goal is reached. Otherwise return to step one and take more uncertain plant representatives.

A. Robust Controller Synthesis

For the controller synthesis step, D-decomposition can usually be used because the characteristic polynomial of the discrete-time system (2) is typically linear in the regulator coefficients (e.g., k_p and k_{ic}).

For our application, assume $R_g \in [0,\ 10]\ \Omega$ and $L_g \in [0,\ 5]$ mH to be the grid impedance uncertainty range and the same root boundary for $t_{s,5\%} \leq 14.3$ ms that was studied in Section III-C. For this uncertainty, the parameter values k_p and k_{ic} are shown in Figure 4b as the red-filled intersection of four root invariant regions corresponding to the four enlarged colored vertices of the uncertainty set in Figure 4a. The values of k_p and k_{ic} inside of each of the four regions in Figure 4b result in zero closed-loop poles outside of the root boundary $z = 0.987\exp(j\Omega)$, which can be seen as a generalization of closed-loop stability (i.e., (3) generalizes $z = \exp(j\Omega)$).

It should be noted that, in some cases (e.g., see [9, Section 11.4]), a controller that is simultaneously stabilizing for all *vertices* of the uncertainty set may not stabilize some other plant representatives inside of the uncertainty set. Therefore, it is advisable to include some samples of uncertain parameters from the depth of the uncertainty set into the set of plant representatives for the robust controller synthesis. In Figure 4a, these additional combinations of L_g and R_g are shown with smaller black dots, and they were also considered when generating the red-filled area in Figure 4b. However, their corresponding extra root-invariant regions are not shown in Figure 4b because they result in no additional constraints.

B. Robustness Analysis

For continuous-time systems, uncertain plant parameters (e.g., L_g and R_g in our example) often enter linearly into the closed-loop characteristic polynomial, which enables the use of D-decomposition for robustness verification. Unfortunately, system discretization causes an exponential dependence of

Authorized licensed use limited to: TU Delft Library. Downloaded on August 13,2020 at 09:18:18 UTC from IEEE Xplore. Restrictions apply.

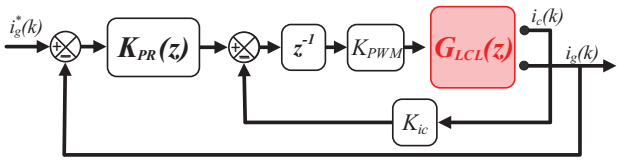

Fig. 6: Block diagram of the control structure in Figure 1

the resulting characteristic polynomial from these physical parameters, thus precluding the direct use of D-decomposition.

Another option is to check the closed-loop system poles for changing uncertain physical parameters. Such check is easy to accomplish if the size of the uncertainty set is rather small. Since the system poles don't jump if the system physical properties are varied continuously, the testing grid in the uncertain parameter space may not be very dense. The closed-loop poles for $k_p = 0.049$, $k_{ic} = 0.042$ and $L_g \in [0,\ 5]$ mH, $R_g \in [0, 10]\ \Omega$ are shown in Figure 5. Thus, the parameters $k_p = 0.049$, $k_{ic} = 0.042$ chosen from the red-filled region in Figure 4b satisfy the Γ-stability specification $z = 0.987\exp(j\Omega)$ for the whole uncertainty range. In Figure 5, higher values of L_g are marked with lighter grayscale colors.

V. Algorithm Implementation

A. Fast Generation of Closed-Loop Systems

The parameter space approach to robust controller design involves computing Γ-stability regions for multiple representatives of the uncertain plant. Therefore, it becomes necessary to generate multiple polynomials in (2) – an operation that may significantly increase the overall computation time.

First, observe that polynomials $U(z)$, $V(z)$, $W(z)$ in (2) can be obtained as closed-loop characteristic polynomials $D(z)$ corresponding to three special values of k_p and k_{ic}:

$$\begin{aligned} W(z) &= D(z, k_p = 0, k_{ic} = 0) \\ U(z) &= D(z, k_p = 1, k_{ic} = 0) - W(z) \\ V(z) &= D(z, k_p = 0, k_{ic} = 1) - W(z) \end{aligned} \tag{8}$$

Second, observe that the control block diagram in Figure 6 consists of the "fixed subsystem" (drawn in black) that can be characterized by the three pairs of k_p and k_{ic} in (8), and the "uncertain subsystem" (filled in red) that is different for every representative of the uncertain plant. Therefore, it is possible to obtain three auxiliary fixed subsystems for the (k_p, k_{ic}) pairs (0, 0), (0, 1), (1, 1). These auxiliary subsystems replicate the black portion of Figure 6. Their output is the VSI voltage signal $v_i(k-1)$ averaged over the sampling period T_s, and their inputs are the VSI output current reference $i^*_{out}(k)$ and the LCL plant signals $i_c(k)$, $i_{out}(k)$. In Figure 8, the z^{-1} block represents the digital regulator time delay of one T_s, and the K_{PWM} block models the VSI as the gain converting the PWM reference signal into $v_i(k-1)$ [10]. For SPWM, $K_{PWM} = V_{dc}/2$. In MATLAB [14], the three auxiliary subsystems can be easily obtained by using the `connect()` function.

Next, it is possible to derive the closed-loop system state-space from the state-space representations of the "fixed subsystem" and "uncertain subsystem" (the derivation is purely algebraic). Representing the "fixed subsystem" of the closed-loop system through three auxiliary subsystems has been discussed above. The ZOH-discretized LCL plant $G_{LCL}(z)$ can be obtained as [13]:

$$\begin{aligned} \mathbf{A_{LCL}} &= \exp(\mathbf{G}T_s), & \mathbf{B_{LCL}} &= \mathbf{G}^{-1}(\exp(\mathbf{G}T_s) - \mathbf{I})\mathbf{H} \\ \mathbf{C_{LCL}} &= \mathbf{C}, & \mathbf{D_{LCL}} &= \mathbf{D} \end{aligned} \tag{9}$$

where $\mathbf{I}$ is the identity matrix, $\mathbf{G}$, $\mathbf{H}$, $\mathbf{C}$, $\mathbf{D}$ are the state, input, output, and feedthrough matrices of the continuous-time state-space plant model, and $\mathbf{A_{LCL}}$, $\mathbf{B_{LCL}}$, $\mathbf{C_{LCL}}$, $\mathbf{D_{LCL}}$ are their discrete-time counterparts. Directly applying (9) is noticeably faster than using the `c2d()` function of MATLAB.

The overall fast generation of closed-loop polynomials can be summarized as follows:

- Generate the three auxiliary fixed subsystems based on the (k_p, k_{ic}) pairs (0, 0), (0, 1), (1, 1).
- Loop over representatives of the uncertain plant:
  1) Discretize the current plant representative using (9).
  2) Use the state-space matrices of the plant and the three auxiliary subsystems to compute the three polynomials $D(z, k_p, k_{ic})$ in (8).
  3) Finally obtain current $U(z)$, $V(z)$, $W(z)$ using (8).

B. Numerical Accuracy Issues

The D-decomposition technique requires the three polynomials $U(z)$, $V(z)$, and $W(z)$ as its inputs. They are obtained through operations with state-space matrices described above and the characteristic polynomial function of MATLAB (i.e., `charpoly()`). These operations have an accuracy close to the machine precision. However, when operating with polynomials (e.g., computing $\Delta_0(x)$, $\Delta_1(x)$, $\Delta_2(x)$), small round-off errors in coefficients may lead to significant deviations of the roots and values of the resulting polynomials. This issue becomes increasingly relevant for high-order polynomials.

To improve the numerical accuracy of operations on polynomials (e.g., polynomial multiplication, polynomial root finding etc.), the Multiprecision Computing Toolbox (MCT) for MATLAB [15] is being used, as computations in variable precision with [15] are not much slower than standard MATLAB computations in the double-precision floating-point format. Alternatively, the Symbolic Math Toolbox of MATLAB can be used, but it is noticeably slower than [15] and thus less suitable for repeated computations of root-invariant regions.

Another alternative is to directly represent the polynomials in x (7) in the Chebyshev polynomial basis. Representing $U''_{re}(x)$, $V''_{re}(x)$, $W''_{re}(x)$, $U''_{im}(x)$, $V''_{im}(x)$, $W''_{im}(x)$ as combinations of Chebyshev polynomials possesses favorable numerical properties on the interval $[-1,\ 1]$, and there are specialized algorithms for polynomials in the Chebyshev basis (e.g., polynomial root finding [16]). Moreover, the Chebfun toolbox for MATLAB [17] exploits the numerical stability of Chebyshev approximations on $[-1,\ 1]$ to extend MATLAB from vectors and matrices to functions. In a nutshell, Chebfun internally represents a function as a high-degree polynomial in the Chebyshev basis and uses specialized algorithms for

Authorized licensed use limited to: TU Delft Library. Downloaded on August 13,2020 at 09:18:18 UTC from IEEE Xplore. Restrictions apply.

such polynomials to perform operations on them. In our experiments, Chebfun performed well with low-order polynomials $D(z)$ in (2) (e.g., 6^{th} order), but produced errors for 12^{th}-order $D(z)$. Thus, the use of MCT or its alternatives is seemingly necessary to produce reliable results for a wide range of control problems.

C. Identification of Root-Invariant Regions

To plot the root-invariant regions as shown in Figure 3, the work window is specified by defining the limits for k_p and k_{ic}: $k_p \in [\underline{k}_p,\ \overline{k}_p]$, $k_{ic} \in [\underline{k}_{ic},\ \overline{k}_{ic}]$. The work window size may be rather large, as the precise analytic description of the borders of root-invariant regions is known.

After the singular values of x have been found, the straight lines corresponding these x_{sng} can be plotted within the work window. The root boundary for non-singular x is defined by (7). To produce more detailed plots, the ranges of x inside which the CRB curve is inside of the work window should be found. This is achieved by solving the system of inequalities:

$$\begin{cases} k_p(x) \geq \underline{k}_p; & k_p(x) \leq \overline{k}_p; \\ k_{ic}(x) \geq \underline{k}_{ic}; & k_{ic}(x) \leq \overline{k}_{ic}; \end{cases} \tag{10}$$

where $k_p(x)$ and $k_{ic}(x)$ are defined by (7). Therefore, inequalities in (10) can be solved through the method of intervals, which again involves polynomial root finding, whereby the roots of Δ_0 are known from the previous search for x_{sng}.

To further improve the CRB plotting accuracy, the extrema of $k_p(x)$ and $k_{ic}(x)$ are found as zeros of $k_p'(x)$ and $k_{ic}'(x)$, which once again involves polynomial root finding. The intervals of x found by solving (10) are subdivided into subintervals by the values of x corresponding to the extrema of $k_p(x)$ and $k_{ic}(x)$, and each subinterval is padded by a sufficient number of x values to produce the plotting grid for the CRB curve.

After the CRB and RRB curves have been plotted in the work window, the next step is to find their intersection points with each other, themselves (self-intersections), and the work window borders. Since the CRB curve is a sequence of line segments and other contours are straight lines, this is a feasible task. Each intersection point is inserted into the datasets of the plotted contours that intersect at it. The resulting plot can be seen as a planar graph, with its vertices being the intersection points and its edges being the CRB and RRB segments between the intersection points. Finding the root-invariant regions becomes equivalent to finding the faces of this planar graph embedded onto a plane. A simple planar embedding face detection algorithm is to start at a graph edge, then select the next edge as the one that make the least angle with the current edge, then repeat this process until a closed contour is identified. All root-invariant regions are detected when each CRB and RRB segment is traversed twice by the face detection algorithm, and each work window border segment is traversed once.

Thus, each root-invariant region is represented by a closed polygon, and it is enough to take only one point in its interior to determine Γ-stability for the whole region. A point grid is generated over the region and the interior point furthermost from the region's borders is taken for testing. Finally, the robust Γ-stability region is computed by intersecting the Γ-stable regions corresponding to all tested representatives of the uncertain plant by using a polygon clipping algorithm.

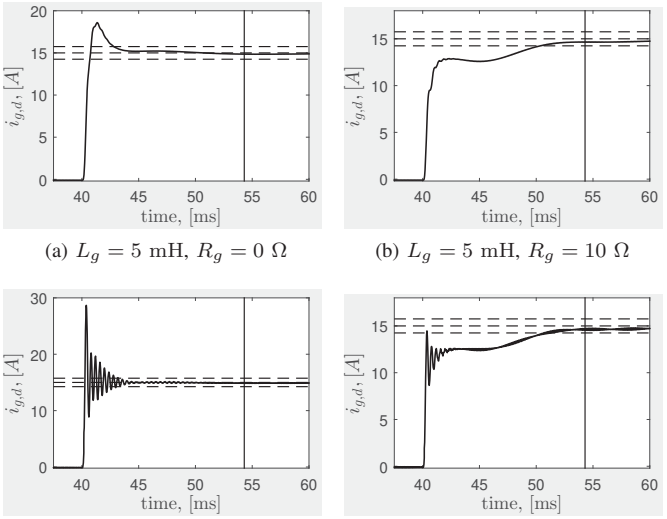

(a) $L_g = 5$ mH, $R_g = 0\ \Omega$ (b) $L_g = 5$ mH, $R_g = 10\ \Omega$

(c) $L_g = 0$ mH, $R_g = 0\ \Omega$ (d) $L_g = 0$ mH, $R_g = 10\ \Omega$

Fig. 7: Time-domain simulations to verify robust settling time

VI. Case Studies

A. Time-Domain Simulations to Verify Robust Settling Time

In Sections III–IV, a robust current regulator has been designed for the LCL filter interfaced VSI with its data given in Table I. The controller synthesis has been focused on robust settling time $t_{s,5\%} < 14.3$ ms for the uncertainty ranges $L_g \in [0,\ 5]$ mH and $R_g \in [0,\ 10]\ \Omega$, and it has resulted in regulator parameter values $k_p = 0.049$, $k_{ic} = 0.042$.

In Figure 7, the robust performance of the designed controller is demonstrated through time-domain simulations using Power System Toolbox of Simulink [14]. A step increase in the controller d-axis current reference $I^*_{g,d}$ from 0 A to 15 A occurs at $t = 40$ ms. The q-axis current reference $I^*_{g,q}$ remains at zero. The associated rotating dq-frame is synchronized with the PCC voltage via a phase-locked loop (PLL) [11]. The closed-loop system response to the described step increase in $I^*_{g,d}$ is shown in black for the vertices of the uncertainty set (see Figure 4a), while the required $t_{s,5\%} = 14.3$ ms is shown as a vertical line and the ± 5 % tolerance band around $I^*_{g,d} = 15$ A is shown with dashed lines. The results in Figure 7 demonstrate the robust performance of the designed regulator in the time domain, which complements the eigenvalue-based robustness analysis of Section IV-B. In Figure 7c, the regulator time response is fast, but poorly damped. Unfortunately, it can be verified with the methodology in this paper that no robust Γ-stable region exists for the given control structure, uncertainty ranges, and the closed-loop poles' damping above $\zeta \approx 0.07$.

In Figure 8, it is further demonstrated that the robust performance is preserved in case of rapid grid impedance

Authorized licensed use limited to: TU Delft Library. Downloaded on August 13,2020 at 09:18:18 UTC from IEEE Xplore. Restrictions apply.

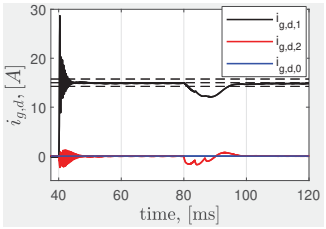

(a) (0 mH, 0 Ω) → (5 mH, 10 Ω)

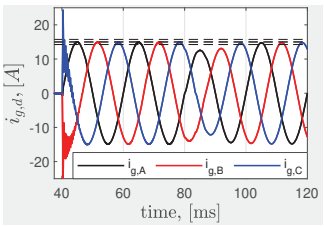

(b) (0 mH, 0 Ω) → (5 mH, 10 Ω)

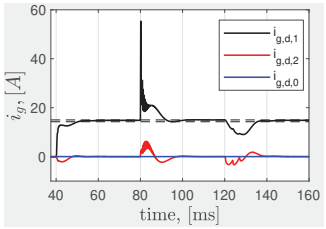

(c) 40 ms 3 phase fault at PCC

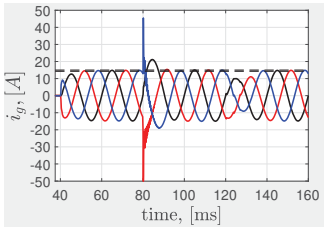

(d) 40 ms 3 phase fault at PCC

Fig. 8: Verification of current regulator transient performance

changes and near short circuit faults. In particular, Figures 7a-7b show the regulator performance for an instantaneous grid impedance increase from zero to (5 mH, 10 Ω) at $t = 80$ ms by displaying the simulated grid output current for this scenario in $dq0$ and ABC reference frames. Similarly, Figures 8c-8d are showing the VSI current response after applying a three phase fault at the PCC from 80 to 120 ms. Some extra simulation results can be found in [18].

B. Extension to Three Parameters

By its nature, the standard D-decomposition method operates in a plane defined by two system parameters. As a straightforward extension, it is possible to apply D-decomposition multiple times, each time varying the value of a third system parameter, and to plot the resulting Γ-stable regions along the third parameter axis. If the third system parameter is varied with a small step size, the resulting 3D image well approximates the Γ-stability region in the three dimensional parameter space.

As an illustrative example, Figure 9 shows the influence of varying the resonant gain k_r of the PR regulator on the robust stability and robust settling time ($t_{s,5\%} < 14.3$ ms). The results in Figure 9 only consider the vertices of the uncertainty domain (see Figure 4a), which implies that they could be too optimistic. On the other hand, it only took about 8-12 minutes to generate Figures 9a–9b, which is a reasonable effort to obtain the initial approximate result.

From Figure 9a, it can be concluded that initial assumption about small influence of k_r on the closed-loop stability is largely valid. In Figure 9a, $k_r = 3, 4, 5, \ldots, 120$, and the cross-sections for various k_r levels remain similar over the whole broad range of k_r values. However, the k_r parameter has a significant influence on robust performance, which is evident from Figure 9b. The range of k_r values that allows for robust settling time $t_{s,5\%} < 14.3$ ms is only around $k_r \in [29,\ 52]$, which is substantially lower than the k_r-range that allows for robust stability (cf. Figure 9a). Moreover, the cross-sections for various k_r levels in Figure 9b differ substantially.

C. Computational Performance

For the 6^{th} order closed-loop system, it took about 5 seconds to compute the robust Γ-stable region in Figure 4 (i.e., for 25 plant representatives). Testing the robust stability by computing closed-loop eigenvalues took only 6.5 seconds for the 2028 plant representatives (see Figure 5).

For a PR regulator with the compensation of 3^{rd}, 5^{th}, 7^{th} harmonics [11], it took about 10 seconds to compute the robustly stable region for the 25 plant representatives. Testing the robust stability of this 12^{th} order closed-loop system for the 2028 LCL filter plant representatives also took 6.5 seconds.

These results were obtained using MATLAB R2019b (64-bit) on a PC with an Intel® Core™-i7 2.2 GHz CPU and 16 Gb of RAM on a single core.

VII. Conclusions and Outlook

The objective of this paper was threefold. First, a concise overview of D-decomposition and parameter space approach was provided. Second, their practicality for the synthesis of low-order digital robust regulators was demonstrated on the example of the VSI current regulation problem. Third, a special attention was given to the implementation issues of parametric controller design methods, including the use of Chebyshev polynomials, algorithm design, and numerical issues. This last point is rarely addressed in the literature, but it is crucial for the successful application of D-decomposition and related techniques. In particular, the double floating-point precision is insufficient to reliably obtain accurate root-invariant regions if the order of the closed-loop system is as low as eight. Nowadays, highly efficient variable precision computation packages are commercially available that allow to increase the resolution of floating-point operations beyond double precision. The numerical robustness can be further improved by working with polynomials represented in the Chebyshev basis. For double precision computations, these techniques are implemented in the Chebfun library [17]; implementing them for variable precision computations is could be a task for future work. As the final takeaway, the presented parametric controller synthesis techniques can be applied to a much broader range of problems than the VSI current regulation that was selected for this study because of the research interests of the first author.

References

[1] L. T. Martins, M. Stefanello, H. Pinheiro, *et al.*, "Current control of grid-tied lcl-vsi with a sliding mode controller in a multiloop approach," *IEEE Trans. Power Electron.*, vol. 34, no. 12, pp. 12356–12367, 2019.

[2] L. A. Maccari, C. L. do Amaral Santini, H. Pinheiro, R. C. L. F. de Oliveira, *et al.*, "Robust optimal current control for grid-connected three-phase pulse-width modulated converters," *IET Power Electron.*, vol. 8, no. 8, pp. 1490–1499, 2015.

[3] G. G. Koch, L. A. Maccari, R. C. L. F. Oliveira, and V. F. Montagner, "Robust h_∞ state feedback controllers based on linear matrix inequalities applied to grid-connected converters," *IEEE Trans. Ind. Electron.*, vol. 66, no. 8, pp. 6021–6031, 2019.

Authorized licensed use limited to: TU Delft Library. Downloaded on August 13,2020 at 09:18:18 UTC from IEEE Xplore. Restrictions apply.

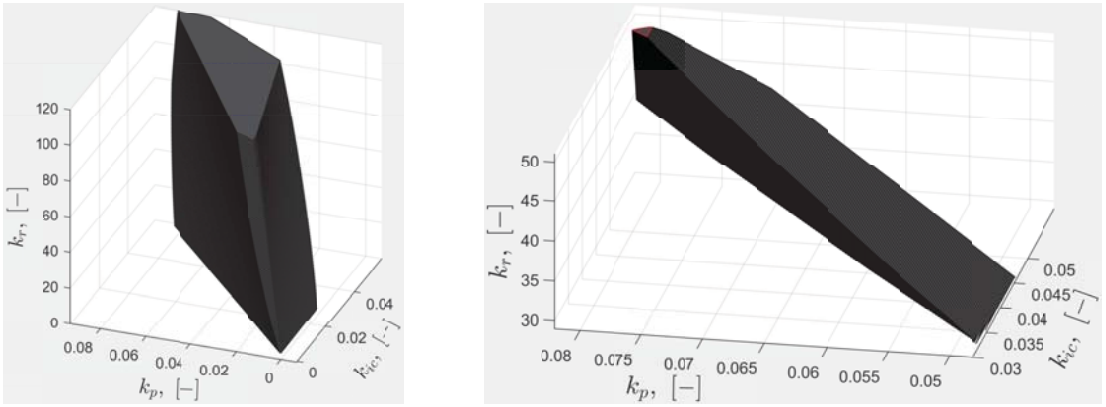

(a) $z = \exp(j\Omega)$ (b) $z = 0.987\exp(j\Omega)$

Fig. 9: Robust Γ-stable regions for 3 parameters

[4] S. Gulur, V. M. Iyer, and S. Bhattacharya, "A dual-loop current control structure with improved disturbance rejection for grid-connected converters," *IEEE Trans. Power Electron.*, vol. 34, no. 10, pp. 10233–10244, 2019.

[5] W. Yao, Y. Yang, Y. Xu, F. Blaabjerg, *et al.*, "Phase reshaping via all-pass filters for robust lcl-filter active damping," *IEEE Trans. Power Electron.*, vol. 35, no. 3, pp. 3114–3126, 2020.

[6] Y. I. Neimark, "Search for the parameter values that make automatic control system stable," *Avtom. Telemekh.*, vol. 9, no. 3, p. 190–203, 1948.

[7] E. N. Gryazina, "The d-decomposition theory," *Avtom. Telemekh.*, vol. 65, no. 12, pp. 1872–1884, 2004.

[8] E. N. Gryazina, B. T. Polyak, and A. A. Tremba, "D-decomposition technique state-of-the-art," *Avtom. Telemekh.*, vol. 69, no. 12, pp. 1991–2026, 2008.

[9] J. Ackermann *et al.*, *Robust Control: The Parameter Space Approach*. London: Springer London, 2 ed., 2002.

[10] D. Pan, X. Ruan, C. Bao, *et al.*, "Capacitor-current-feedback active damping with reduced computation delay for improving robustness of lcl-type grid-connected inverter," *IEEE Trans. Power Electron.*, vol. 29, no. 7, pp. 3414–3427, 2014.

[11] R. Teodorescu, M. Liserre, and P. Rodriguez, *Grid converters for photovoltaic and wind power systems*. Wiley-IEEE Press, 2 ed., 2011.

[12] M. Liserre, F. Blaabjerg, and S. Hansen, "Design and control of an lcl-filter-based three-phase active rectifier," *IEEE Trans. Ind Appl.*, vol. 41, no. 5, pp. 1281–1291, 2005.

[13] G. F. Franklin, D. J. Powell, and M. L. Workman, *Digital Control of Dynamic Systems*. Addison-Wesley, 3 ed., 1998.

[14] MATLAB R2019b (9.7.0). Nattick, MA: The MathWorks Inc., 2019.

[15] Multiprecision Computing Toolbox for MATLAB 4.7.0. Yokohama, Japan: Advanpix LLC., 2020.

[16] J. P. Boyd, "Computing the zeros, maxima and inflection points of chebyshev, legendre and fourier series: solving transcendental equations by spectral interpolation and polynomial rootfinding," *J Eng Math*, vol. 56, no. 3, pp. 203–219, 2006.

[17] Z. Battles and L. N. Trefethen, "An extension of matlab to continuous functions and operators," *SIAM J. Sci. Comput.*, vol. 25, no. 5, pp. 1743–1770, 2004.

[18] I. Tyuryukanov, J. Wang, and A. Monti, "Design of a novel robust current controller for grid-connected inverter against grid impedance variations," *International Journal of Electrical Power & Energy Systems*, vol. 110, pp. 454–466, 2019.

Authorized licensed use limited to: TU Delft Library. Downloaded on August 13,2020 at 09:18:18 UTC from IEEE Xplore. Restrictions apply.